RSC Advances

PAPER

View Article Online
View Journal | View Issue

Cite this: *RSC Adv.*, 2018, **8**, 6870

On the morphological, structural and electrochemical properties of entangled Cu-filled carbon nano-onions†

X. Zhang,[a] D. Medranda,[a] J. Borowiec,[a] K. Yan,[c] J. Zhang,[c] S. Wang[b] and F. S. Boi *[a]

Received 20th November 2017
Accepted 3rd February 2018

DOI: 10.1039/c7ra12626c

rsc.li/rsc-advances

In this work we demonstrate an advanced chemical vapour synthesis approach in which the synthesis of Cu-filled carbon nano-onions (CNOs) is achieved by direct sublimation and pyrolysis of a not previously used precursor, namely chloro(1,5-cyclooctadiene)copper(I) dimer. The cross-sectional morphology and filling-ratio of the as grown CNOs were characterized by detailed transmission electron microscopy (TEM), high resolution TEM analyses, Fourier transform and lattice profile analyses. The structural graphitic arrangement and electronic properties of the CNOs were then investigated by means of X-ray diffraction and absorption spectroscopy. The electrochemical impedance spectroscopy and cyclic voltammetry of presented structures were also investigated and reveal a high electrical resistance. Finally the electrochemical performances of this type of CNOs were compared with those of another type of CNOs filled with different metal-carbide materials.

Introduction

Carbon nano-onions (CNOs) are frequently defined as fullerene-like structures consisting of $60N^2$ carbon atoms (N being the number of carbon layers) arranged in concentric shells with a graphitic arrangement.[1–5] In the last decade these structures have become an important focus of research thanks to their excellent physical/chemical properties, which include high surface areas in the order of 30–500 $m^2\ g^{-1}$,[6–8] high thermal stability, giant capacitance[4,10] and high conductivity (in the order of 10 S cm^{-2}).[6] In addition to these characteristics, high mechanical properties have been recently demonstrated.[9] Applications of CNOs include energy storage,[10,15] dielectric,[11,12] additives for aerospace,[14] miniaturised fuel cells[13] and others.[15–17] As electrode materials, CNOs have been reported to provide fast charge/discharge rates. However due to the low specific energy parameters reported up to now, more work is necessary to tailor the properties of these nanostructures for possible energy storage applications. Thanks to the strong chemical stability CNOs have been recently considered suitable also for the encapsulation of specific materials of interest and their protection from interactions with the external environment.[18,19] Indeed the CNOs shells can chemically passivate the chosen encapsulated material (specifically metals/alloys) and limit its interaction with other chemical species that are present in the external environment. An important attention has been focused on the encapsulation of ferromagnetic nanocrystals (*i.e.* Fe-based interstitial and substitutional alloys) within the CNOs core due to the high coercivities that these materials can exhibit when fabricated in small dimensions.[20,21] In addition to the cases above, the encapsulation of copper (Cu) inside carbon materials (mostly CNOs and carbon nanotubes) has shown great promise for technological applications thanks to its good electrical and thermal conducting properties, and to its low binding energy to carbon (*ca.* 0.1 eV).[22–26] Encapsulation of Cu inside carbon materials has been reported to possibly lead to important nanoscale applications such as spot-welding. In addition Rheostatlike Behavior and Femtogram Cu Mass Transport have been recently reported.[22] In particular these kind of structures have been reported to (1) behave like nano-scale rheostat like switches with the electrical resistance strongly dependent on the copper filling ratio and (2) exhibit/possess an electrically driven femtogram Cu mass transport (at a speed of *ca.* 0.5 fg s^{-1}) in condition of low applied voltages. Such unique properties in the electrical resistance of Cu-filled nanotubes could have important implications also on the electrical and electronic properties of other carbon materials when filled with Cu nanocrystals. Interestingly Cu-filled CNOs have been previously synthesised by using: (I) DC arc discharge, or (II) carbon-ion implantation into copper substrates.[27,28] Instead high temperature experiments performed between copper dichloride dihydrate ($CuCl_2 \cdot 2H_2O$) and calcium carbide (CaC_2) did not show Cu-encapsulation.[29] Further work is therefore necessary to better understand the conditions of Cu

[a]College of Physical Science and Technology, Sichuan University, Chengdu, China. E-mail: f.boi@scu.edu.cn
[b]Analytical and Testing Centre, Sichuan University, Chengdu, China
[c]School of Chemistry and Chemical Engineering, Huazhong University of Science and Technology, Wuhan, China

† Electronic supplementary information (ESI) available. See DOI: 10.1039/c7ra12626c

encapsulation in CNOs and investigate the properties of these nanostructures in presence of these type of crystals.

Here we demonstrate an advanced chemical vapour synthesis (CVS) approach in which the synthesis of Cu-filled CNOs is achieved by direct sublimation and pyrolysis of a not previously used precursor, namely chloro(1,5-cyclooctadiene) copper(I) dimer. The cross-sectional morphology and filling-rate of the as grown CNOs is characterized by detailed transmission electron microscopy (TEM) and high resolution TEM analyses. The structural and electronic arrangement is then investigated by means of absorption spectroscopy and X-ray diffraction (XRD). The electrochemical impedance spectroscopy (EIS) and cyclic voltammetry (CV) measurements of these structures are also investigated and reveal their resistive properties.

Experimental

Synthesis

Cu-filled CNOs were fabricated by sublimation and pyrolysis of 50 mg of as purchased chloro(1,5-cyclooctadiene)copper(I) dimer, in an Ar flow of 11 mL min^{-1} on the top of quartz boats positioned inside a quartz tube reactor of length 1.5 metres. A one-zone electrical furnace was used for reaching the desired temperature of pyrolysis (temperature of 990 °C). The sublimation temperature was of approximately 700 °C. The reaction was started by sliding the furnace in the reaction zone along a rail system. The used reaction time was 25 min. Note that attempts of using lower evaporation temperatures with the use of a preheater did not show successful evaporation of the precursor. A fast cooling method was used to bring the samples to room temperature. Cooling times in the order of 20 min were achieved by removing the furnace along a rail system. See scheme in Fig. 1 for direct visualization of the CVS approach.

Characterization

TEM and HRTEM investigations were performed using a 200 kV American FEI Tecnai G^2F20 fitted with field emission gun. XRD analyses were performed with a Empyrean Panalytical diffractometer (Cu Kα with $\lambda = 0.154$ nm).

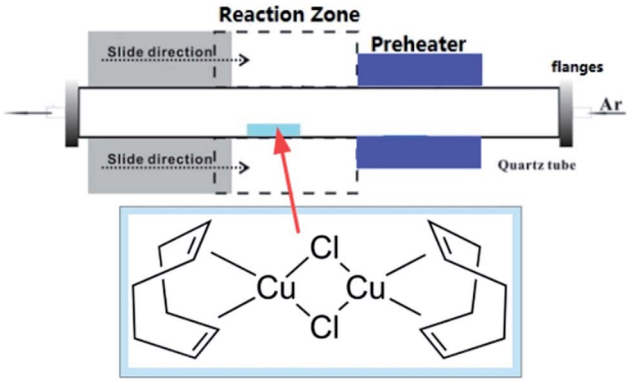

Fig. 1 Scheme showing the experimental CVS setup used for the fabrication of the Cu-filled CNOs.

Raman spectroscopy experiments were performed with an Andor SR-500i with a wavelength of 532 nm, acquisition time of approximately 100 seconds per sample-area. X-ray photoelectron spectroscopy (XPS) analyses were performed with an Escalab 250Xi (see ESI†).

Electrochemical impedance spectroscopy measurements were performed on a CHI660A workstation (Chenhua Instrument Co. Ltd., China) in a conventional three-electrode system. A modified electrode, a saturated calomel electrode (SCE) and platinum wire were employed as the working, reference and counter electrode, respectively. EIS measurements were performed in 5 mmol L^{-1} $K_3[Fe(CN)_6]/K_4[Fe(CN)_6]$ aqueous solution with 0.1 mol L^{-1} KCl as the supporting electrolyte in the frequency range from 100 MHz to 100 kHz.

Potassium-hexacyanoferrate(II)trihydrate ($K_4[Fe(CN)_6]\cdot 3H_2O$), potassium-hexacyanoferrate(III) ($K_3[Fe(CN)_6]$) and potassium chloride (KCl) were provided by Sinopharm Chemical Reagent Co. Ltd. (Shanghai, China). UV-Vis absorption was recorded by using a Hanon i5 UV-Vis Spectrophotometer (Jinan Hanon Instruments Co., Ltd., China).

Results and discussion

The cross-sectional morphology of the as grown CNOs was firstly revealed by TEM micrographs as shown in Fig. 2A and B. Curiously the as grown CNOs were found with an entangled-like morphology which resembles that of recently reported Fe_3C-filled CNOs-buckypapers obtained by pyrolysis of ferrocene.[20] Such a morphological arrangement may imply the presence of a high number of van der Waals interactions between the neighbouring CNOs.

The presence of Cu within the CNOs-core was also verified by the presence of a clear dark-contrast in the core of numerous CNOs, as shown in Fig. 2B. Further analyses of these structures were then performed in HRTEM mode in the attempt to gather further information on the structural arrangement of both the CNOs and the encapsulated crystals.

As shown in Fig. 3A and B the presence of distorted-like graphitic layers with lattice spacing in the order of 0.39 nm was found. Furthermore, analyses of the inner CNOs-core confirmed the presence of crystalline Cu. As shown in Fig. 3C, the fast Fourier transform (FFT) of the area enclosed within the red square revealed the presence of a lattice spacing of 0.20 nm which could be ascribed to the 111 reflection of fcc Cu.

In order to further investigate the level of crystalline graphitization of the CNOs further analyses were performed in HRTEM mode. As shown in Fig. 4 these analyses revealed the presence of a variable level of graphitization within the CNOs structure (see pink arrow in Fig. 4A and HRTEM image in Fig. 4B) as well as a variable filling rate. Typical examples of hollow CNOs found within the as grown sample are shown by the green arrow in Fig. 4A and in HRTEM mode in Fig. 5 where a high detail of an empty CNOs-core is shown. Note in this case the presence structural defects which could be ascribed to the fast cooling rate imposed by the quench (note dark areas in Fig. 5 indicating the presence of stress in the CNO structure).

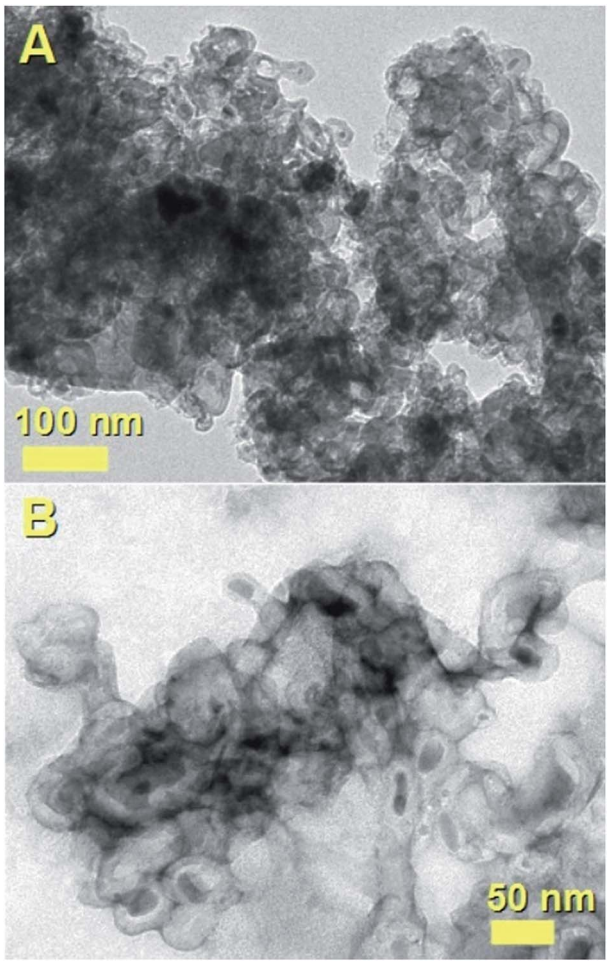

Fig. 2 TEM analyses in A and B showing the cross-sectional morphology of the as grown CNOs arranged in an entangled bucky-paper-like morphology.

Further analyses of graphitic-layer quality in the structure of the CNO shown in Fig. 5 were then considered by means of HRTEM analyses at higher magnification. As shown in Fig. 6 and 7 these analyses revealed the presence of both 002 and 004 graphitic reflections, as shown by the FFT analyses (of the area within the red square) in the inset of Fig. 7 and profile analyses in Fig. 6.

In the attempt to better evaluate the level of graphitic arrangement within the CNOs, additional TEM analyses were performed in other parts of the sample deposited on the TEM grid. As shown in Fig. 8 and 9 these analyses revealed the presence of another type of CNO structure coated by amorphous-like carbon layers (see red arrow in Fig. 8). Surprisingly HRTEM analyses in these type of CNOs revealed also the presence of a Cu_2O phase, as shown in Fig. 9 by the pink arrow (lattice profile measurement) and by the FFT analyses of the area within the red square. These analyses revealed the presence of the following lattice spacings: 0.32 nm (red circles), 0.25 nm (blue circles) and 0.20 nm (orange circles) which could be ascribed to the 110, 111 and 200 reflections of Cu_2O with space group $Pn\bar{3}m$.

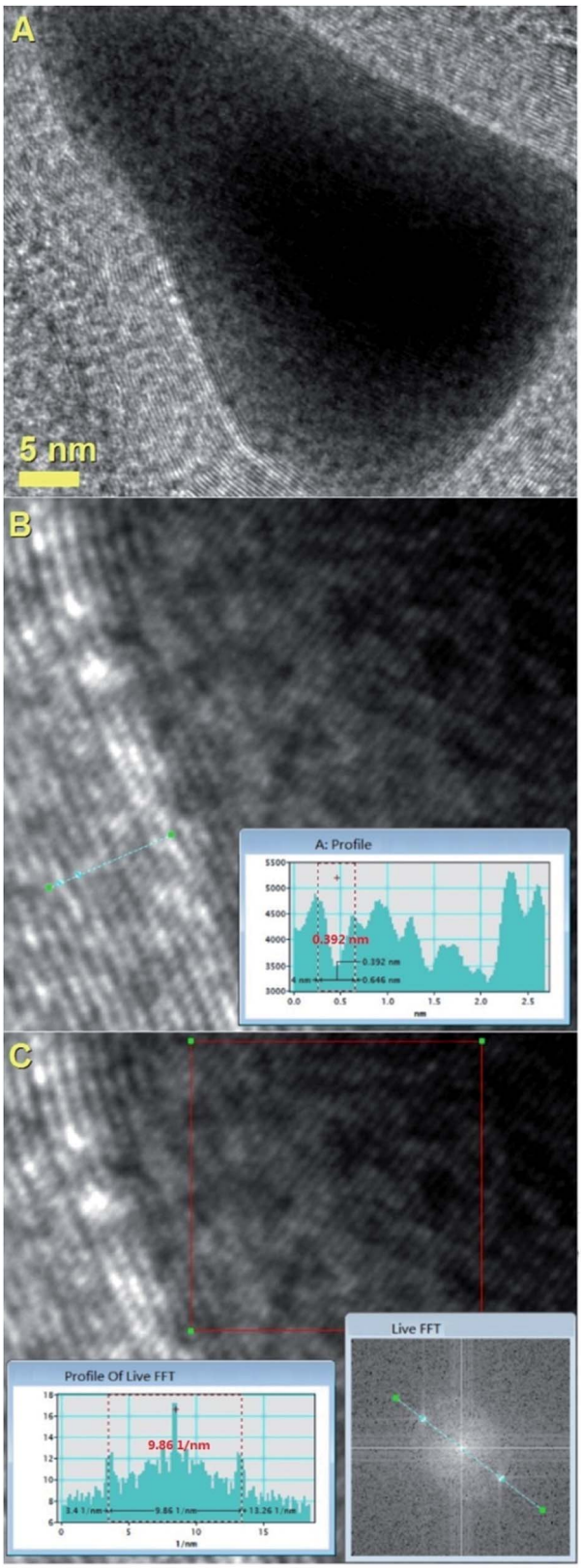

Fig. 3 HRTEM micrograph of a typical Cu filled CNO. In B the presence of graphitic layers is shown through profiling of the HRTEM image. In C the presence of Cu in the CNO core is shown by FFT analyses of the area within the red square.

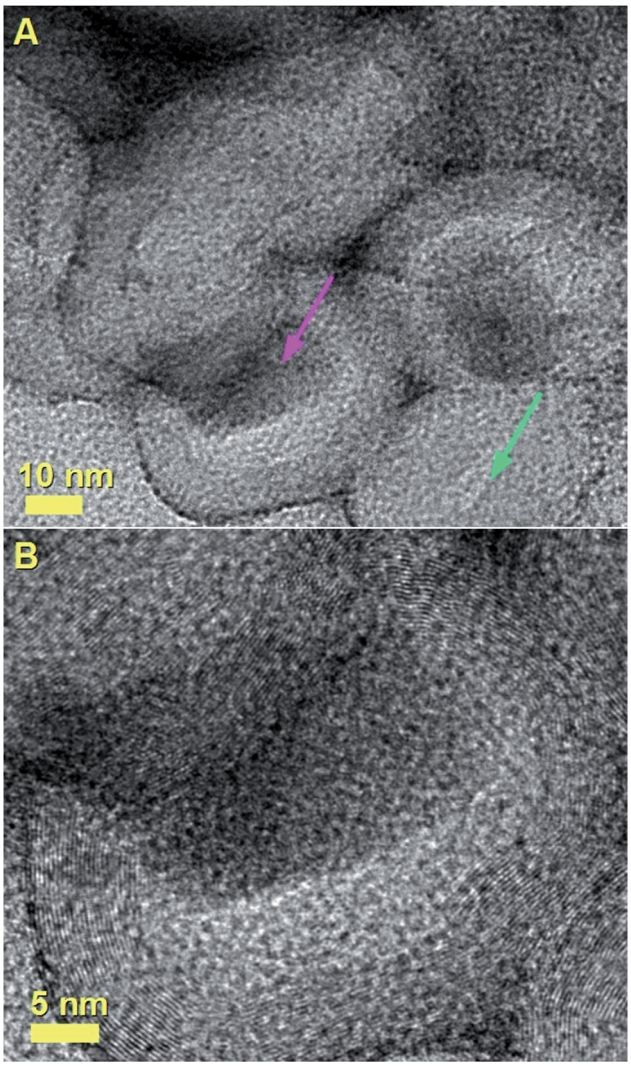

Fig. 4 TEM analyses of typical Cu-filled and hollow CNOs comprised in the buckypaper-like structure shown in Fig. 2.

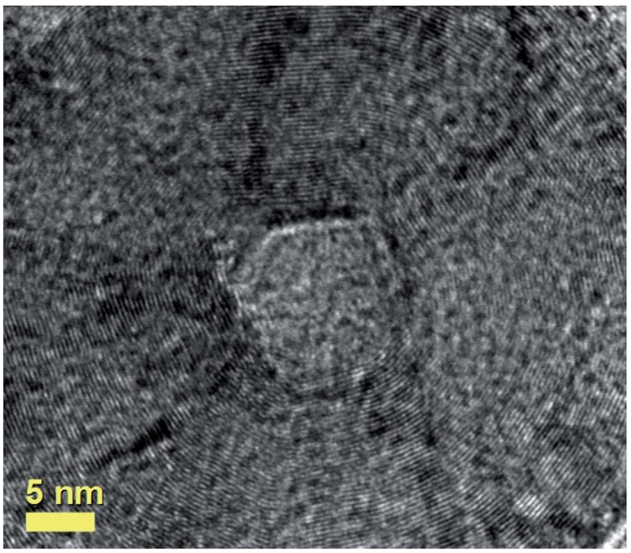

Fig. 5 HRTEM micrograph showing with high detail an example of hollow CNO.

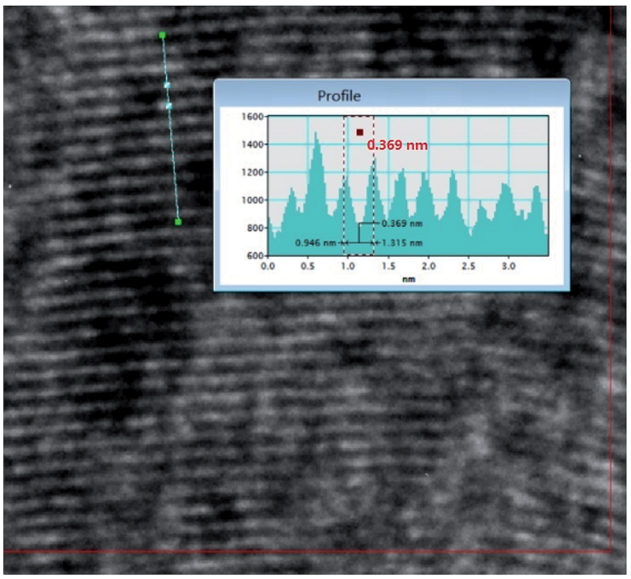

Fig. 6 Profile analyses of the graphitic layers comprised in the hollow CNO previously shown in Fig. 5.

In the attempt to verify these interpretations the use of XRD analysis was then considered. As shown in Fig. 10 these analyses revealed the presence of large quantities of Cu and small quantities of Cu_2O, confirming the above TEM analyses (see also ESI† for additional XPS, Raman spectroscopy and Rietveld refinement analyses). The presence of a graphitic arrangement within the CNOs structure was also confirmed by a small peak in the region of 26.03° 2θ.

The structural quality of the as grown CNOs was then analysed further by means of UV absorption spectroscopy. As shown in Fig. 11 these analyses revealed the presence of a single absorption feature in the region of 220 nm which could be ascribed to the π-plasmonic characteristic electronic arrangement of the CNOs. The observation of this feature confirms the presence of CNOs within the as grown sample. However, the presence of an unusual broadening was also found, as shown in Fig. 11B. The broad shape of this characteristic absorption feature could be possibly attributed to the variable level of graphitization within the structure of the produced CNOs.

Attention was then focused on the electrochemical properties of the as grown CNOs. Note that the performances of Cu-filled CNOs were also compared with those of another type of CNOs filled with different metal-carbide materials (Fe_3C).[20] The electrochemical properties of the bare glassy carbon electrode (GCE), Fe_3C filled CNOs and Cu/Cu_2O filled CNOs modified GCE were investigated by cyclic voltammetry (CV), at a scan rate of 50 mV using the $K_3[Fe(CN)_6]/K_4[Fe(CN)_6]$ redox probe. The cyclic voltammograms are shown in Fig. 12A and B. As it can be seen, in the case of GCE a single pair of peaks (indicated as A_1/C_1 in Fig. 12A and B) appears due to redox reactions of the $K_3[Fe(CN)_6]/K_4[Fe(CN)_6]$ redox couple (curve a). A significant

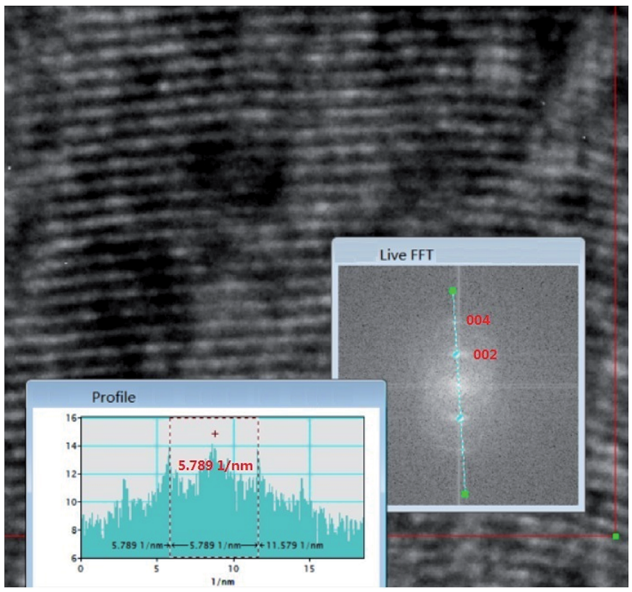

Fig. 7 FFT analyses of the graphitic layers comprised in the hollow CNO previously shown in Fig. 5.

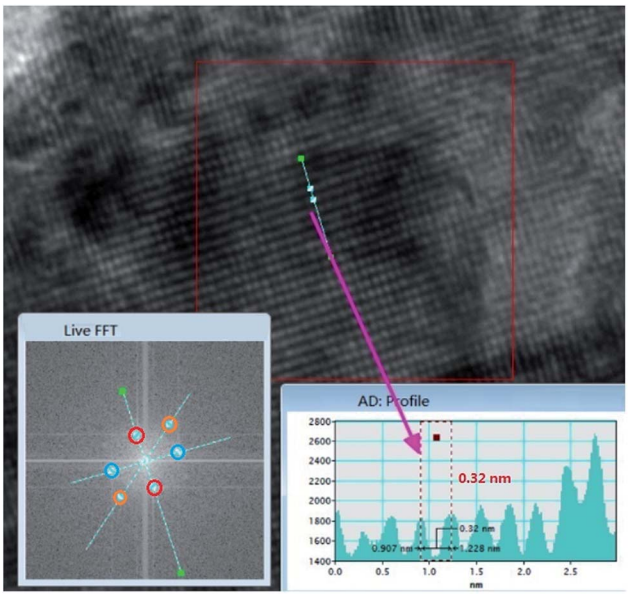

Fig. 9 HRTEM micrograph, profile and FFT analyses (right and left insets) of the Cu_2O crystal shown in Fig. 8.

increase of the peak current response (faster electron transport properties) related to that process, can be seen in the case of Fe_3C filled CNOs modified GCEs (curve b in Fig. 12A, peaks A_2/C_2). However, additional pair of peaks (Fig. 12A, peaks A_3/C_3) is apparent on the cyclic voltammograms of the Fe_3C filled CNOs/GCE. Those peaks can be assigned to the oxidation (forward sweep, peak A_3) and reduction (reverse sweep, peak C_3) processes of Fe^{2+}/Fe^{3+} redox couple.[30]

This indicates that iron oxide species (*e.g.* Fe_3O_4, Fe_2O_3) that originate from the oxidation of Fe_3C or are a secondary products obtained during synthesis, are present on the sample surface. In contrast with that located on the surface, the Fe in the form of Fe_3C located in the core of CNOs should be both physically shielded from the electrolyte and chemically stabilized by graphitic layers. Similarly, in the case of Cu/Cu_2O filled CNOs/GCE the cyclic voltammogram (curve c in Fig. 12B) is composed of several peaks, indicating additional electrochemical processes occurring on the electrode surface. As indicated, in the forward scan direction (anodic scan) two peaks assigned as A_2 and A_3 can be assigned to oxidation of Cu^0 to Cu_2O, and Cu_2O to complex hydrous CuO (represented by $CuO_x(OH)_{2-2x}$, where $0 \leq x \leq 1$).[31–33] The oxidation reactions are followed by reduction process of hydrous CuO to Cu_2O in the reverse scan (cathodic scan), which is represented by appearance of cathodic peak assigned as C_3.[32] The oxidation and reduction peaks at higher potentials, indicated as A_4 and C_3 (curve c in Fig. 12B), respectively, are due to redox reactions of

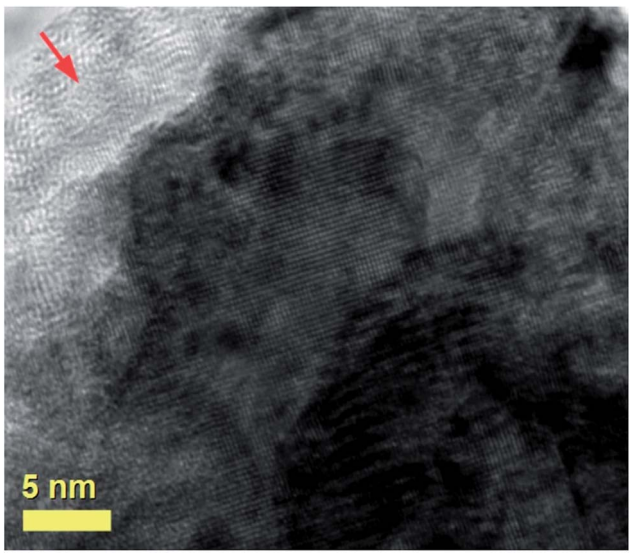

Fig. 8 TEM micrograph of the second type of CNO characterized by amorphous-like carbon layers surrounding a Cu_2O core.

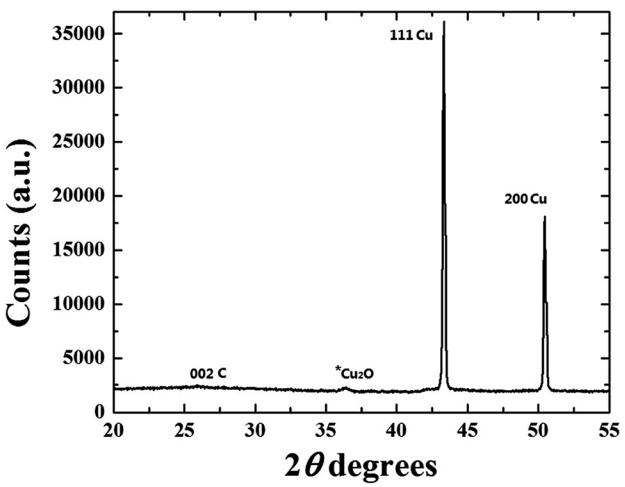

Fig. 10 XRD pattern of the as grown Cu-filled CNOs.

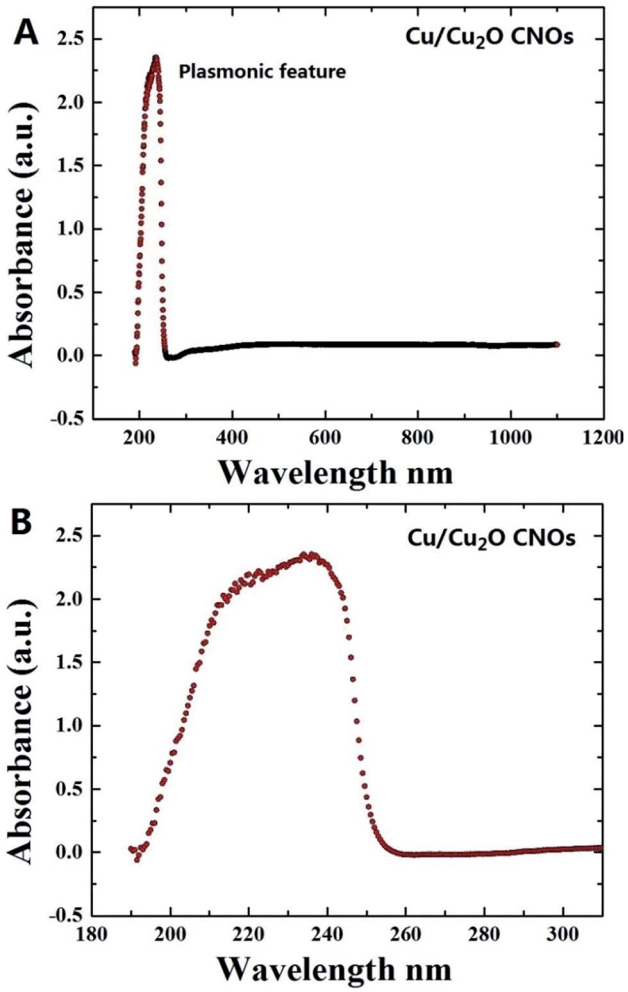

Fig. 11 UV spectroscopy analyses of the as grown Cu-filled CNOs.

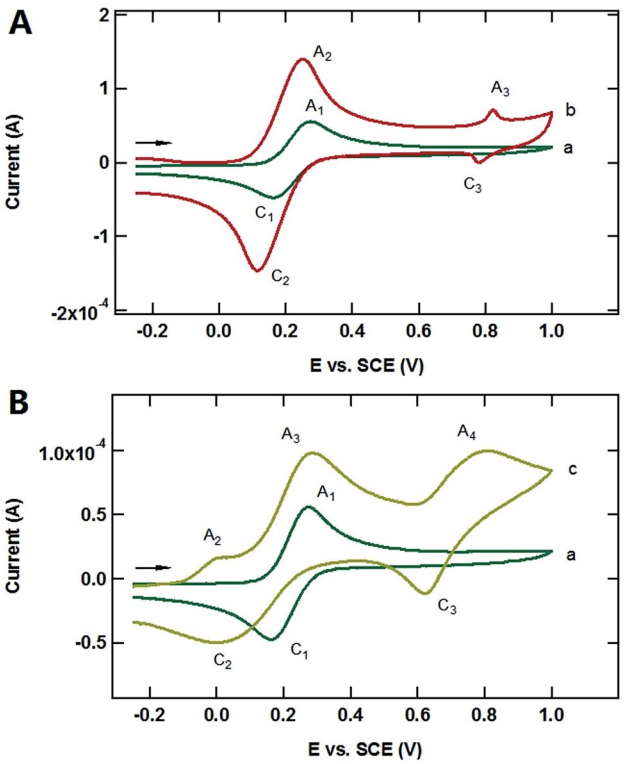

Fig. 12 Cyclic voltammograms of (A) GCE (a) and Fe_3C filled CNOs/GCE (b); and (B) GCE (a) and Cu/Cu_2O filled CNOs/GCE (c), recorded in 5 mmol L^{-1} $K_3[Fe(CN)_6]/K_4[Fe(CN)_6]$ solution containing 0.1 mol L^{-1} KCl. Scan rate: 50 mV s^{-1}. Arrow indicates the scan direction.

Table 1 Cyclic voltammetry results obtained for GCE, Fe_3C filled CNOs/GCE and Cu/Cu_2O filled CNOs/GCE

Electrode	Peak[a]	E [V]	I [A]	ΔE_p [V]
GCE	A_1	0.276	5.91×10^{-5}	0.116
	C_1	0.160	-5.60×10^{-5}	
Fe_3C CNOs/GCE	A_2	0.249	1.40×10^{-4}	0.136
	C_2	0.113	-1.56×10^{-4}	
	A_3	0.823	2.00×10^{-5}	0.042
	C_3	0.781	-1.35×10^{-5}	
Cu/Cu_2O CNOs/GCE	A_2	0.008	2.07×10^{-5}	—
	A_3	0.283	1.02×10^{-4}	0.275
	C_2	0.003	-5.96×10^{-5}	
	A_4	0.808	1.04×10^{-4}	0.185
	C_3	0.623	-2.12×10^{-5}	

[a] Peak annotation corresponds to assignment given in Fig. 12A and B.

the $K_3[Fe(CN)_6]/K_4[Fe(CN)_6]$ redox couple.[34] Moreover, from the CVs we can observe the increase of the peak potential values for the redox reactions (ΔE_p) of 0.116, 0.136 and 0.185 V for GCE, Fe_3C and Cu/Cu_2O filled CNOs modified GCE, respectively. The increase of peaks potentials separation indicates that those materials do not possess catalytic properties toward carried out electrochemical reaction. Characteristic values obtained from CV measurements are collected in Table 1.

In order to gain insight on the intrinsic electrochemical properties of the Fe_3C and Cu/Cu_2O filled CNOs modified GC electrodes, electrochemical impedance spectroscopy (EIS) measurements were carried out within the probed frequency range of 100 MHz to 100 kHz. Fig. 13 illustrates the Nyquist plots of the impedance of the modified GCEs. It can be clearly observed that the impedance curves show similar features, and are composed of an arc and followed by a slanted line at low frequency. While in the high frequency region, the intercept of the semicircle on the real axis of the Nyquist spectrum represents the solution resistance (R_e) which can be correlated to the ohmic resistance of the electrolyte in the system, the contacts and connections. The semicircles in the high and mid frequency regions are attributed to the charge transfer resistance between the interfaces of the electrode materials and electrolyte. The electron transfer which occurs in these regions during the charge/discharge processes is conceptualized by an interfacial charge transfer resistance (R_{ct}). Beyond the semicircle region, the Nyquist spectrum shows a long tail in the low frequency region, which can be associated to the Warburg resistance of the electrode. As dictated in Fig. 13, it is apparent that the diameters of the Nyquist semicircles are varied for the examined electrodes, and increase in order Fe_3C filled CNOs/GCE, GCE and Cu/Cu_2O filled CNOs/GCE. The charge transfer

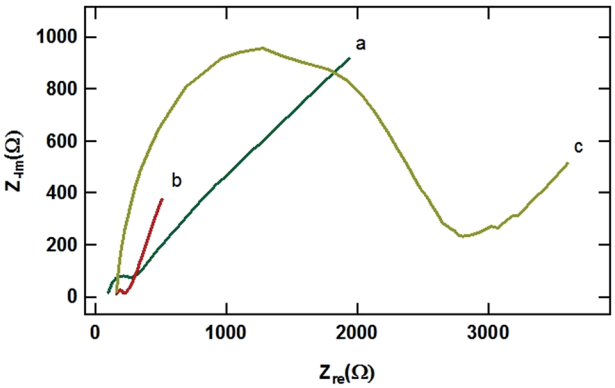

Fig. 13 Nyquist plot of the (a) GCE, (b) Fe_3C filled CNOs/GCE and (c) Cu/Cu_2O filled CNOs/GCE in 5 mmol L^{-1} $K_3[Fe(CN)_6]/K_4[Fe(CN)_6]$ solution containing 0.1 mol L^{-1} KCl. The frequency range was from 100 MHz to 100 kHz, and the amplitude 5 mV.

resistance (R_{ct}) values for Fe_3C filled CNOs/GCE, GCE and Cu/Cu_2O filled CNOs/GCE were estimated to be 53.4, 229.2 and 2391.7 Ω, respectively; implying the relatively low internal resistivity for the electrode that is modified with Fe_3C CNOs. From these results, it is apparent that the modification of the GCE with Cu/Cu_2O filled CNOs exhibits the highest R_{ct} value, consistent with the largest diameter of the Nyquist semicircle within the high frequency region. An increase in the value of R_{ct} implies that the modification decreases the conductivity of the electrode, and increases the charge transfer resistance of the $K_3[Fe(CN)_6]/K_4[Fe(CN)_6]$ redox couple. This phenomenon can be understood by referring to the composition of Cu/Cu_2O filled CNOs material where a variable level of graphitization is present.

Conclusion

In conclusion we have demonstrated an advanced CVS approach in which the synthesis of Cu-filled carbon nanoonions (CNOs) is achieved by direct sublimation and pyrolysis of a not previously used precursor, chloro(1,5-cyclooctadiene)copper(I) dimer. The properties of the as grown CNOs were then characterized in detail by means of TEM, HRTEM, FFT, XRD, absorption spectroscopy, EIS and CV. Particularly the CV and EIS analyses show that these type of CNOs exhibit resistive properties which appear to be strongly dependent on the crystalline quality of the graphitic carbon shells. Instead no influence of the encapsulated Cu/Cu_2O crystals on these characteristics was found.

Conflicts of interest

There are no conflicts to declare.

Acknowledgements

We acknowledge Prof. Gong Min for his continuous support in this research work. We are also grateful for the NSFC 11404227.

References

1 D. Ugarte, *Nature*, 1992, **359**, 707–709.
2 H. W. Kroto, J. R. Heath, S. C. O. Brien, R. F. Curl and R. E. Smalley, *Nature*, 1985, **318**, 162–163.
3 L. Hultman, S. Stafstrom, Z. Czigany, J. Neidhardt, N. Hellgren, I. F. Brunell, *et al.*, *Phys. Rev. Lett.*, 2001, **87**, 225503.
4 N. Sano, H. Wang, M. Chhowalla, I. Alexandrou and G. A. J. N. Amaratunga, *Nature*, 2001, **414**, 506–507.
5 M. Chhowalla, H. Wang, N. Sano, K. B. K. Teo, S. B. Lee and G. A. J. Amaratunga, *Phys. Rev. Lett.*, 2003, **90**, 155504.
6 R. Borgohain, J. Yang, J. P. Selegue and D. Y. Kim, *Carbon*, 2014, **66**, 272–284.
7 P. Z. Si, Z. D. Zhang, D. Y. Geng, C. Y. You, X. G. Zhao and W. S. Zhang, *Carbon*, 2003, **41**, 247–251.
8 A. Palkar, F. Melin, C. M. Cardona, B. Elliott, A. K. Naskar, D. D. Edie, *et al.*, *Chem.–Asian J.*, 2007, **5**, 625–633.
9 R. Pawlak, S. Kawai, S. Fremy, T. Glatzel and E. Meyer, *ACS Nano*, 2011, **5**, 6349–6354.
10 D. Pech, M. Brunet, H. Dorou, P. H. Huang, V. Mochalin, Y. Gogotsi, *et al.*, *Nat. Nanotechnol.*, 2010, **5**, 651–654.
11 J. Macutkevic, J. Banys, S. Moseenkov, V. Kuznetsov, N. Nunn and O. Shenderova, *Polym. Compos.*, 2005, 2084–2092.
12 D. W. M. Lau, D. G. McCulloch, N. A. Marks, N. R. Madsen and A. V. Rode, *Phys. Rev. B*, 2007, **75**, 233408.
13 A. S. Rettenbacher, B. Elliott, J. S. Hudson, A. Amirkhanian and L. Echegoyen, *Chem.–Eur. J.*, 2006, **12**, 376–387.
14 X. H. Chen, F. M. Deng, J. X. Wang, H. S. Yang, G. T. Wu, X. B. Zhang, *et al.*, *Chem. Phys. Lett.*, 2001, **336**, 201–204.
15 M. Zeiger, N. Jäckel, V. N. Mochalin and V. Presser, *J. Mater. Chem. A*, 2016, **4**, 3172–3196.
16 O. Mykhailiv, H. Zubyk and M. E. Plonska-Brzezinska, *Inorg. Chim. Acta*, 2017, **468**, 49–66.
17 Y. Zheng and P. Zhu, *RSC Adv.*, 2016, **6**, 92285–92298.
18 R. S. Ruoff, D. C. Lorents, B. Chan, R. Malhotra and S. Subramoney, *Science*, 1993, **259**, 346–348.
19 F. Banhart, E. Hernandez and M. Terrones, *Phys. Rev. Lett.*, 2003, **90**, 185502.
20 F. S. Boi, J. Guo, G. Xiang, M. Lan, S. Wang, J. Wen, *et al.*, *RSC Adv.*, 2017, **7**, 845.
21 F. S. Boi, S. Ivaturi, S. Wang and X. Zhang, *Carbon*, 2017, **120**, 392–396.
22 D. Golberg, P. M. F. J. Costa, M. Mitome, S. Hampel, D. Haase, C. Mueller, A. Leonhardt and Y. Bando, *Adv. Mater.*, 2007, **19**, 1937.
23 A. A. Setlur, J. M. Lauerhaas, J. Y. Dai and R. P. H. Chang, *Appl. Phys. Lett.*, 1996, **69**, 345.
24 G. Y. Zhang and E. G. Wang, *Appl. Phys. Lett.*, 2003, **82**, 1926.
25 X. R. Ye, Y. Lin, C. Wang and C. M. Wai, *Adv. Mater.*, 2003, **15**, 316.
26 D. Haase, S. Hampel, A. Leonhardt and B. Büchner, *Surf. Coat. Technol.*, 2007, **201**, 9184.
27 X. F. Zhang, X. L. Dong, H. Huang, D. K. Wang, B. Lv and J. P. Lei, *Nanotechnology*, 2007, **18**, 275701.
28 T. Cabioch, J. P. RiviZxe, M. Jaouen, J. Delafond and M. F. Denanot, *Synth. Met.*, 1996, **77**, 253–256.

29 H. Fu-Dong, Y. Bin and B. Yu-Jun, *J. Phys. Chem. C*, 2011, **115**, 8923–8927.
30 A. S. Adekunle, S. Lebogang, P. L. Gwala, T. P. Tsele, L. O. Olasunkanmi, F. O. Esther, D. Boikanyo, N. Mphuthi, J. A. O. Oyekunle, A. O. Ogunfowokan and E. E. Ebenso, *RSC Adv.*, 2015, **5**, 27759–27774.
31 M. Seo, X. C. Jiang and N. Sato, *Werkst. Korros.*, 1988, **39**, 583.
32 R. Babic, M. Metikos-Hukovic and A. Jukic, *J. Electrochem. Soc.*, 2001, **148**, B146–B151.
33 Y. Wan, Y. Zhang, X. Wang and Q. Wang, *Electrochem. Commun.*, 2013, **36**, 99–102.
34 L. Berisha, A. Maloku, E. Andoni and T. Arbneshi, *Am. J. Anal. Chem.*, 2014, **5**, 308–315.